



**Relative stability of the FCC and HCP polymorphs with interacting polymers**

Journal:	<i>Soft Matter</i>
Manuscript ID:	SM-ART-10-2014-002191.R1
Article Type:	Paper
Date Submitted by the Author:	31-Oct-2014
Complete List of Authors:	Mahynski, Nathan; Princeton University, Chemical & Biological Engineering Kumar, Sanat; Columbia University, Chemical Engineering Panagiotopoulos, Athanassios; Princeton University, Chemical & Biological Engineering

# Relative stability of the FCC and HCP polymorphs with interacting polymers†

Nathan A. Mahynski,<sup>a</sup> Sanat K. Kumar,<sup>b</sup> and Athanassios Z. Panagiotopoulos<sup>\*a</sup>

Received Xth XXXXXXXXXXXX 20XX, Accepted Xth XXXXXXXXXXXX 20XX

First published on the web Xth XXXXXXXXXXXX 200X

DOI: 10.1039/b000000x

Recent work [Mahynski *et al.*, *Nat. Commun.*, 2014, **5**, 4472] has demonstrated that the addition of long linear homopolymers thermodynamically biases crystallizing hard-sphere colloids to produce the hexagonal close-packed (HCP) polymorph over the closely related face-centered cubic (FCC) structure when the polymers and colloids are purely repulsive. In this report, we investigate the effects of thermal interactions on each crystal polymorph to explore the possibility of stabilizing the FCC crystal structure over the HCP. We find that the HCP polymorph remains at least as stable as its FCC counterpart across the entire range of interactions we explored, where interactions were quantified by the reduced second virial coefficient,  $-1.50 < B_2^* < 1.01$ . This metric conveniently characterizes the crossover from entropically to energetically dominated systems at  $B_2^* \approx 0$ . While the HCP relies on its octahedral void arrangement for enhanced stability when  $B_2^* > 0$ , its tetrahedral voids produce a similar effect when  $B_2^* < 0$  (*i.e.* when energetics dominate). Starting from this, we derive a mean-field expression for the free energy of an infinitely-dilute polymer adsorbed in the crystal phase for nonzero  $B_2^*$ . Our results reveal that co-solute biasing of a single polymorph can still be observed in experimentally realizable scenarios when the colloids and polymers have attractive interactions, and provide a possible explanation for the experimental finding that pure FCC crystals are elusive in these binary mixtures.

## 1 Introduction

The face-centered cubic (FCC) and hexagonal close-packed (HCP) crystals are closely related polymorphs which are often formed simultaneously by crystallizing hard spheres. These polymorphs generally occur together in nature because the free energy difference between the two is on the order of  $0.001k_{\text{B}}T$  per sphere, with entropy marginally favoring the FCC structure.<sup>1–3</sup> The similarity in free energy results from the fact that these structures have an identical coordination number ( $z = 12$ ) and optimal packing fraction for spheres of  $\pi\sqrt{2}/6 \approx 0.74$ .<sup>4</sup> Consequently, it can take months or years for mixed crystals to fully anneal into the more stable FCC structure.<sup>5</sup> In the same vein, crystallization of hard spheres is often difficult to study experimentally because of experimental factors such as size polydispersity,<sup>6,7</sup> gelation and vitrification,<sup>7,8</sup> and the stress of terrestrial gravity<sup>9</sup> which present barriers to the production of crystals with any significant long-range order. Such order is a necessity for a wide range of technological applications including photonic band gap materials, optical filters, and lasers.<sup>10–12</sup> Recently, we demonstrated a unique approach to selecting only one of the two competing polymorphs by amplifying the difference in free energy between them by adding a co-solute such as a linear homopolymer.<sup>13</sup>

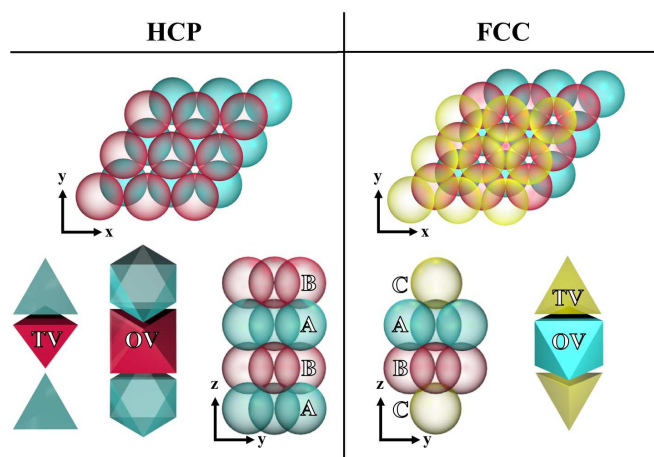


**Fig. 1** Close-packed crystals have two polymorphs, the face-centered cubic (FCC) and hexagonal close-packed (HCP) structures. In the HCP crystal, planes of hexagonally packed spheres are stacked in a repeating ABAB pattern such that planes are staggered to form octahedral void (OV) spaces that stack vertically and share faces with one another. The remaining space is covered by pairs of tetrahedral voids (TV) which also share faces. However, the FCC crystal has ABC stacking symmetry which eclipses each OV with TVs and neither void type shares any faces with their same type.

The key feature of our approach is that the co-solute's free energy is controlled by the distribution of free volume in the crystal (*cf.* Fig. 1). In both polymorphs, layers of hexagonally packed spheres are stacked on each other so that a second layer (B) eclipses half of the trigonal voids formed between tangent triplets of spheres in the layer below (A). In the FCC crystal, the third layer is rotated  $60^\circ$  relative to the first, and thus eclipses the other half of the trigonal voids producing an ABC stacking

† Electronic Supplementary Information (ESI) available: [details of any supplementary information available should be included here]. See DOI: 10.1039/b000000x/

<sup>a</sup> Department of Chemical and Biological Engineering, Princeton University, Princeton, NJ 08544, USA. E-mail: azp@princeton.edu

<sup>b</sup> Department of Chemical Engineering, Columbia University, New York, NY 10027, USA

---

pattern; however, in the HCP crystal, the third and fourth layers simply repeat the first two producing an ABAB stacking pattern. In both cases, all the free volume in each crystal can be divided into voids shaped like one of two platonic solids, octahedrons or tetrahedrons, which are formed by treating the centers of mass of the spheres as vertices as illustrated in Fig. 1. Out of the stacking plane, both octahedral voids (OV) and tetrahedral voids (TV) are situated directly on top of themselves in the HCP crystal because of the ABAB symmetry, whereas in the FCC crystal each OV is capped by TVs owing to the ABC stacking pattern.

Thus, when a sufficiently long linear homopolymer is adsorbed in a HCP crystal it can distribute itself across neighboring OVs, while in the FCC crystal a similarly sized polymer would be forced into an OV-TV pair. Since an OV cavity contains roughly 6 times the volume as a TV, the pairs of OVs provide significantly more free volume (entropy) for the polymer.<sup>13</sup> Thus, for low polymer densities in the athermal case, where entropy alone determines the system's free energy, the HCP crystal is always favored over the FCC. This difference occurs when the polymer's radius of gyration is on the order of the colloid diameter, defining an entropic length scale in the crystal for the binary mixture,  $l_s$ . The effect has been generalized to linear block copolymers to show that engineering the polymer architecture is an effective way to select which polymorph will be the most thermodynamically stable in different systems, at least when the polymer concentration in the crystal phase is low.<sup>13</sup>

Our prior findings have significant implications on the study of depletion-induced colloidal crystallization. Depletion is a phenomenon whereby a mixture containing size asymmetric species separates as a result of entropy.<sup>14–16</sup> The aggregation of the larger species disproportionately increases the amount of free volume in the bulk for the smaller one(s) thereby increasing the overall entropy of the system. This is often used as a driving force to produce fluid-fluid phase separation and to crystallize suspensions of colloids.<sup>8,15–18</sup> Athermal linear homopolymers are common well-studied depletants.<sup>13,19–23</sup> However, additional factors can be adjusted to fine tune the behavior of such a depletant. For instance, the importance of attractive interactions between the polymer and colloids is of particular interest since in many experimental situations some amount of attraction between the polymer and colloids is expected due to dispersion forces. The introduction of a thermal length scale,  $l_u$ , which characterizes this interaction is expected to create competition with the entropic one, potentially producing nontrivial results. While a great deal of effort has been focused on understanding the fluid phase behavior of colloid-polymer mixtures and the dispersion characteristics in polymer nanocomposites,<sup>24–29</sup> to our knowledge a study of the relative stability of the colloidal crystal phases in the presence of attractive polymers has not yet been undertaken. Here we elucidate the role of thermal interactions between linear homopolymers and colloids in determining the relative stability of the two close-packed polymorphs to investigate the applicability of the void-leveraging technique in more realistic and experimentally representative scenarios.

The rest of this article is organized as follows: in Section 2 we describe our model and simulation methodology, in Section 3 we discuss our results pertaining to the relative stability of the two polymorphs, and we conclude in Section 4.

---

## 2 Methods

### 2.1 Simulations

We employed Monte Carlo (MC) simulations to measure the total excess chemical potential,  $\mu_{\text{tot}}^{\text{ex}}$ , of a single chain adsorbed in each crystal morphology.<sup>30</sup> A comparison of results obtained in each polymorph has previously shown  $\mu_{\text{tot}}^{\text{ex}}$  to be a reliable predictor of the most stable structure in dense binary mixtures of colloids and polymers since it qualitatively mirrors results obtained from molecular dynamics (MD) simulations of crystallization from these mixtures.<sup>13</sup> Presumably, this is because the polymer density in the crystal is low. When crystals were formed in those MD simulations, the polymer concentration observed in the crystal phase was quite dilute, consistent with theoretical predictions, and therefore the interaction between different polymers is negligible; thus, we can reasonably take the behavior of a single adsorbed polymer to be representative of the ensemble of adsorbed chains. However, these MD simulations are very time consuming, often taking months of wallclock time to produce conclusive results, even when accelerated on graphics processing units, whereas the MC sampling of the excess chemical potential requires mere days. This makes it an invaluable approach for screening a wide range of conditions.

Polymers were modeled as fully flexible “Kremer-Grest” linear chains of beads,<sup>31</sup> each having a diameter of unity,  $\sigma_{\text{m}} = 1$ , and colloids as large spheres of diameter,  $\sigma_{\text{c}} \geq 6.45$ . The size ratio  $\sigma_{\text{c}}/\sigma_{\text{m}} = 6.45$  is the smallest that still allows monomers to penetrate triplets of tangent colloids in the close-packed crystals. Using a smaller size ratio would trap a polymer in a specific void inhibiting sampling of other interstices in the crystal. The FCC lattice was generated in a periodic cubic simulation box with edges of length  $L = 2\sqrt{2}(\sigma_{\text{c}} + 0.12)$ , containing a total of 32 colloids. The HCP lattice was generated in a periodic box with dimensions  $\langle L_x, L_y, L_z \rangle = \langle 4(\sigma_{\text{c}} + 0.12), 4\sqrt{3/4}(\sigma_{\text{c}} + 0.12), 4\sqrt{2/3}(\sigma_{\text{c}} + 0.12) \rangle$ , containing a total of 64 colloids. Colloids were initialized on their respective lattices with an additional spacing of 0.12 between nearest neighbors because we chose the interaction between them to be a translated purely repulsive Lennard-Jones potential (*cf.* eq. 4) rather than that of perfectly hard spheres. This additional gap results in crystals with zero internal energy and configurational pressure, and allows the polymer to move between different voids more easily. The marginal softness of this potential mimics real colloids, which are usually capped with surface ligands, better than a simple hard sphere potential. Over the course of a simulation the colloidal positions were held fixed. Polymers were grown bead-by-bead inside each type of crystal by repeatedly performing test insertions of a new monomer on the end of the chain at regularly spaced intervals and measuring the energy cost,  $U_{\text{ins}}$ , of doing so.

The fully inserted portion of a chain was relaxed according to the Metropolis criterion in the canonical (NVT) ensemble. Relaxation moves allow the chain to fully explore configurational space and include local displacements of monomers, displacements of the entire polymer’s center of mass, and regrowth of the chain from either of its ends by Rosenbluth sampling.<sup>32</sup> These moves typically occurred with a 7:2:1 ratio, respectively. The ensemble averaged Boltzmann factor to insert a new “ghost” monomer on the end of the chain is used to calculate the incremental excess chemical potential:

$$\mu_i^{\text{ex}} = -k_{\text{B}}T \ln \langle \exp(-U_{\text{ins}}/k_{\text{B}}T) \rangle \quad (1)$$

At the end of the sampling, one such configuration is selected and the last bead is formally inserted on the end of the chain, then the process is repeated for the next monomer. It has been shown that it is formally correct to obtain the total chemical potential of a polymer chain of arbitrary length,  $M$ , by summing the previous incremental chemical potentials.<sup>30</sup>

$$\mu_{\text{tot}}^{\text{ex}} = \sum_{i=1}^M \mu_i^{\text{ex}} \quad (2)$$

Bonds are ergodically sampled by choosing a length for the next ghost position according to their energy distribution.

$$P_{\text{bond}}(r) \sim 4\pi r^2 \exp(-U_{\text{bond}}(r)/k_{\text{B}}T) \quad (3)$$

As such, bonding contributions to the insertion energy are not included in eq. 1, but would otherwise simply result in a linear translation of the chemical potential akin to simply selecting a different reference state, and thus were disregarded. New insertions were typically attempted after several thousand relaxation moves. Between  $10^7$  and  $7.5 \times 10^7$  relaxation moves were performed for each monomer fully inserted in the system before the chain was appended with a new monomer. All simulations were repeated between 10 and 60 times to obtain good statistics.

## 2.2 Simulation Potentials

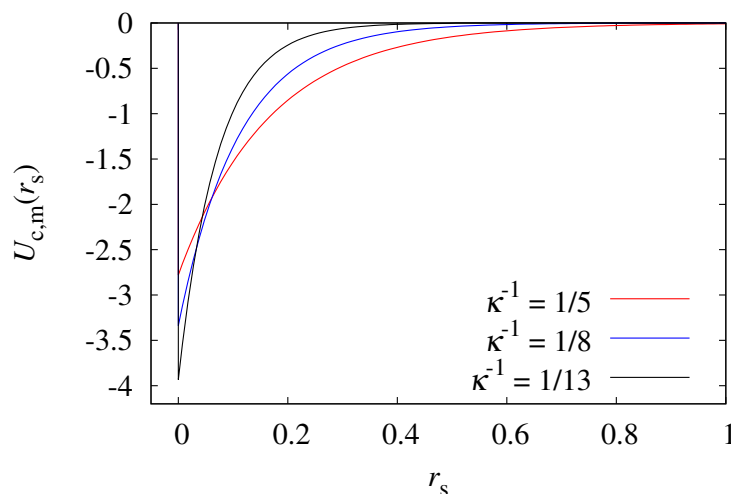


**Fig. 2** Example pair potential between a colloid and monomer for  $\sigma_c = 6.45$ ,  $B_2^* = 0.00$  as a function of surface-to-surface separation distance,  $r_s$ . The strength of the interaction is adjusted to keep  $B_2^*$  constant as the decay length,  $\kappa^{-1}$ , is also changed.

**Table 1** Interaction types between the monomer segments and colloids used in the majority of our simulations, unless otherwise stated, for  $\sigma_c = 6.45$  with their accompanying parameters.

Type	Equation	$\kappa^{-1}$	$\epsilon/k_B T$	$B_2^*$
Lennard-Jones	(4)		1.00	1.01
Yukawa	(6)	1/5	1.92	0.50
Yukawa	(6)	1/5	2.50	0.19
Yukawa	(6)	1/5	2.78	0.00
Yukawa	(6)	1/5	3.00	-0.19
Yukawa	(6)	1/5	4.00	-1.50

The interaction between unbonded (non-neighboring) monomer segments on a polymer chain is given by a translated purely repulsive Lennard-Jones potential which is truncated and shifted to zero at its minimum:

$$U_{i,j}(r) = \begin{cases} \infty & r \leq \Delta \\ 4\epsilon \left( \left( \frac{1}{r-\Delta} \right)^{12} - \left( \frac{1}{r-\Delta} \right)^6 \right) + \epsilon & \Delta < r \leq \Delta + r_{\text{cut}} \\ 0 & r > \Delta + r_{\text{cut}}, \end{cases} \quad (4)$$

where  $r_{\text{cut}} = 2^{1/6}$ . This potential is also used to describe the interaction between colloids and monomer beads in the purely repulsive limit. The linear shift is defined as  $\Delta = (\sigma_i + \sigma_j)/2 - 1$ , for any pair of species with diameters  $\sigma_i$  and  $\sigma_j$ , such that the slope of the potential is fixed for all pairs as they begin to overlap regardless of their individual diameters. Bonds between neighboring monomer segments are represented by supplementing eq. 4 with the finitely extensible nonlinear elastic (FENE) potential.

$$U_{\text{bond}}(r) = -\frac{1}{2}kr_0^2 \ln \left( 1 - \left( \frac{r}{r_0} \right)^2 \right) \quad (5)$$

We employed the standard Kremer-Grest model where  $k = 30.0$  and  $r_0 = 1.5$  to avoid bond crossing.<sup>31</sup> To investigate the influence of attractive interactions between the monomer segments and colloids we introduced a Yukawa-like potential between the two as an alternative to eq. 4:

$$U_{c,m}(r) = \begin{cases} \infty & r \leq \Delta + 1 \\ -\frac{\epsilon}{r-\Delta} \exp(\kappa(\Delta + 1 - r)) & \Delta + 1 < r \leq r_{\text{cut}} + \Delta \\ 0 & r > r_{\text{cut}} + \Delta \end{cases} \quad (6)$$

This potential is a useful model for both screened electrostatic and simple dispersion interactions. Unless otherwise stated, we chose  $\kappa^{-1} = 1/5$  and  $r_{\text{cut}} = 2$  for  $\sigma_c = 6.45$  (cf. Fig. 2). These choices result in a potential that is short enough in range to avoid significant many-body interactions even when a monomer is confined in a TV. The reduced second virial coefficient,  $B_2^*$ , was used to characterize the interaction between the monomers and colloids.

$$B_2^* = -\frac{3}{(1 + \Delta)^3} \int_0^{\Delta + r_{\text{cut}}} [\exp(-U_{\text{c,m}}(r)/k_{\text{B}}T) - 1] r^2 dr \quad (7)$$

We initially explored a range of  $B_2^*$  from  $-1.50 \leq B_2^* \leq 1.01$  for  $\sigma_{\text{c}} = 6.45$  at fixed  $\kappa^{-1}$  where the monomers and colloids ranged from being strongly attractive to having purely repulsive interactions. Table 1 summarizes the interaction potentials we investigated and the corresponding  $\epsilon$  values. For comparison, we subsequently explored the effects of changing both the range,  $\kappa^{-1} = 1/5, 1/8, 1/13$  ( $r_{\text{cut}} = 2.0, 1.8, 1.5$ , respectively), and strength,  $\epsilon$ , of thermal interactions independently for  $\sigma_{\text{c}} = 6.45, 8.00, 9.50, 11.00$  (see Supplementary Information for more details†).

### 3 Results and Discussion

#### 3.1 Effect of attractive interactions

Figure 3(a) depicts the incremental excess chemical potential for each bead grown on a linear chain inside each polymorph for  $\sigma_{\text{c}} = 6.45$ . We repeated detailed simulations for  $\sigma_{\text{c}} = 9.50$  as well, but found no qualitative differences (*cf.* SI). Computational limitations prevented us from obtaining accurate results at larger ratios between the colloid and monomer diameter, so we would like to emphasize to the reader that our results are strictly valid only in the limit of nanoscale colloids since  $\sigma_{\text{m}}$  is typically on the order of 1 nm for many polymers.<sup>33</sup> However, we expect our results to be qualitatively representative over a broader range of colloidal sizes. We focus on three representative cases where  $B_2^* = 1.01, 0.00$ , and  $-1.50$  which summarize the different qualitative behavior regimes that occur as a result of the introduction of attractive thermal interactions between the monomers and colloids. The data for  $B_2^* = 1.01$  were obtained for the case where the monomers and colloids were purely repulsive as reported in ref. 13 and are described by eq. 4. In this case, the incremental chemical potential of each bead is directly related to the free volume it can access inside each crystal.

$$\exp\left(\frac{-\mu_i^{\text{ex}}}{k_{\text{B}}T}\right) = P_{\text{ins}} \sim \frac{V_{\text{free}}}{V_{\text{tot}}} \quad (8)$$

In the case of perfectly hard spheres, eq. 8 becomes an equality, and in the case of infinitely small monomers the right hand side (free volume fraction) becomes  $1 - \pi\sqrt{2}/6 \approx 0.26$ . For monomers of a finite size, this is an upper bound. Once the first bead has been successfully inserted, the next bead is placed somewhere in the immediate vicinity with an orientation chosen at random at a distance proportional to the bonding energy. Because the insertion trial locations of the second bead are conditional on the location of the first, the free volume fraction available to the second bead is often higher than for the first. This is because first beads that are successfully placed are often located in large cavities. Thus, in their immediate vicinity, a substantial fraction of the volume located within one bond length ( $r_0 = 1.5$ ) of the first bead is usually free to accommodate the second, and its incremental chemical potential is consequently lower. Since this “substantial fraction” is generally in excess of  $\sim 26\%$  the

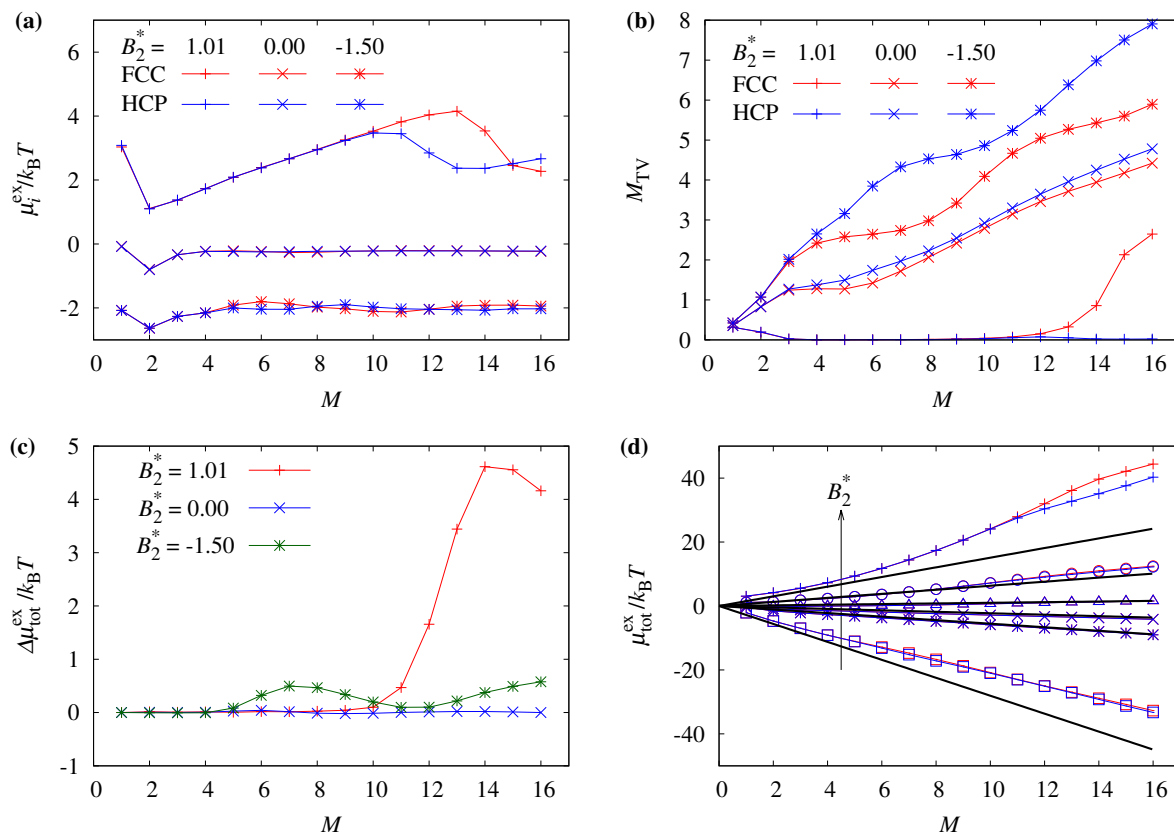


**Fig. 3** (a) Incremental excess chemical potential of each bead for a chain of length  $M$  at  $B_2^* = 1.01, 0.00,$  and  $-1.50$  where  $\sigma_c = 6.45$ . Results from inside the FCC polymorph are given in red, the HCP in blue. (b) Average number of monomers in TVs,  $M_{\text{TV}}$ , for a chain of total length  $M$  in each polymorph for various  $B_2^*$ . Error bars encompassing 95% confidence are smaller than symbol size. (c) Difference in the total excess chemical potential of a polymer (*cf.* eq. 2) between the FCC and HCP polymorphs,  $\Delta\mu_{\text{tot}}^{\text{ex}} = \mu_{\text{tot}}^{\text{ex}}(\text{FCC}) - \mu_{\text{tot}}^{\text{ex}}(\text{HCP})$ . (d) Total excess chemical potential for a chain of length  $M$  for all  $B_2^*$  reported in Table 1. Solid black lines are mean-field theory results given by eq. 13, and red and blue curves correspond to the FCC and HCP polymorphs, respectively.

incremental chemical potential of the second bead always appears lower than the first. However, as the chain continues to grow, monomers progressively fill these cavities increasing  $\mu_i^{\text{ex}}$  for subsequent beads.

When the monomers are purely repulsive, both with one another and with the colloids in the crystal, the system is dominated by entropic effects. The chain quickly senses that the OV is entropically favored over the TVs due to the asymmetry of their cavity volumes, and almost exclusively occupies an OV when the chain is short (*cf.* Fig. 3(b)). As the chain grows, its confinement increases monotonically until it perforates the OV it occupies. This is the point at which differences between the two polymorphs become apparent. In the HCP crystal, the growing chain can simply spread into one of its two large neighboring OVs, whereas in the FCC crystal the chain is forced to traverse highly confining TVs before it can reach the next OV. This produces the loop in Fig. 3(a), the characteristic rise and plateau in the number of monomers occupying TVs,  $M_{\text{TV}}$ , in Fig. 3(b), and the large positive difference in the total free energy of the polymer between the two polymorphs in Fig. 3(c).

Once thermal interactions between the monomer beads and colloids are introduced, entropy no longer exclusively determines

the free energy of the polymer inside each polymorph. Two additional, qualitatively unique, scenarios emerge. First, when the interaction is sufficient that  $B_2^* = 0.00$ , the shape of the incremental chemical potential curve becomes flat and is essentially identical for both polymorphs. Indeed, the difference in the total chemical potential between the FCC and HCP states was not distinguishable to within 95% confidence. Furthermore, the occupancy of the TVs also becomes qualitatively different. As shown in Fig. 3(b) the two polymorphs are almost identical over the range of chain lengths we investigated, and the curves rise almost linearly. Second, when the monomer beads and colloids are strongly interacting ( $B_2^* = -1.50$ ), the incremental chemical potential begins to exhibit oscillations as the overall chain length increases. The amplitude of each subsequent oscillation is not sufficient to destroy the preceding ones, however, and an oscillatory difference in  $\Delta\mu_{\text{tot}}^{\text{ex}}$  emerges remaining positive over the range of  $M$  investigated. This is accompanied by similar oscillations in  $M_{\text{TV}}$  which appear to be complementary between the two polymorphs (*cf.* Fig. 3(b)).

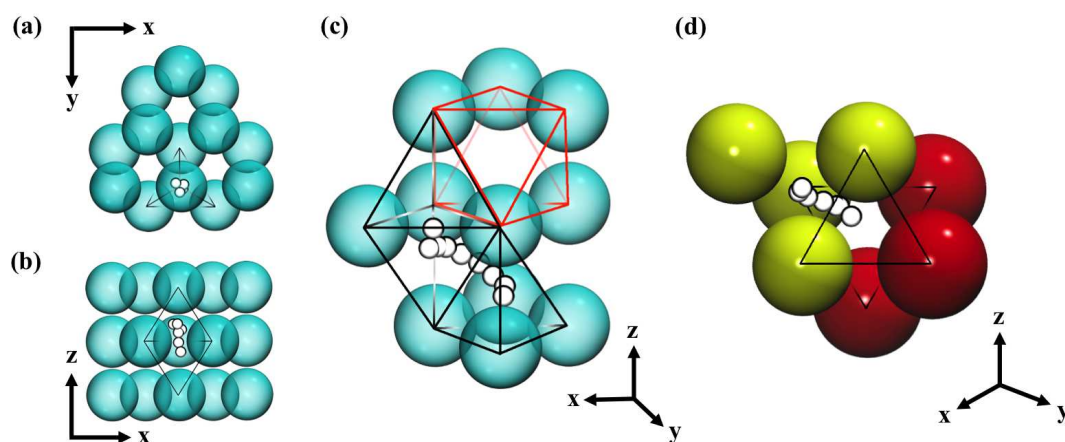


**Fig. 4** Characteristic polymer conformations when thermally adsorbed in the HCP (a)-(c), and FCC (d) crystals. The relative size of the colloids has been reduced for visual clarity. (a) and (b) depict the same polymer ( $M = 6$ ) viewed from different planes. As suggested by Fig. 3(b) the polymer is entirely inside a pair of face-sharing TVs (indicated by black lines). (c) As the chain becomes longer ( $M = 9$ ), it spreads from one pair of TVs to another, crossing over an OV in doing so. The TVs are traced out in black, while one OV is indicated in red. The chain depicted enters the OV directly below the one indicated, which is omitted for clarity. (d) In the FCC crystal, pairs of TVs do not share faces, and thus a chain must enter an OV once it has filled a TV completely. The TV is indicated in yellow, and contributes three of the six colloids which form the OV; the rest are indicated in red. The OV faces in neighboring stacking planes are traced out with black lines to give some perspective.

In order to understand the cause of these effects one must reconsider the different void distributions between the polymorphs. Each scenario is characterized by its own set of conformational “modes” which define a confined polymer’s behavior in these voids. For instance, when  $B_2^* = 1.01$  it is the relative placement of the large OVs which determine the difference in polymer chemical potential between the polymorphs, while the TVs play only an implicit role, serving as barriers which separate their larger counterparts. Figure 4(a) depicts the HCP crystal observed from the  $z$ -plane in which the OVs are the visible cavities. Hence, the OV-OV connections in the HCP polymorph provide a mode for the adsorbed polymer to be placed along, lowering its free energy relative to the FCC polymorph which lacks such a mode.

However, as thermal interactions begin to factor into the free energy of an adsorbed polymer, the TVs no longer play a passive role. As the monomer segments and colloids begin to interact in an energetically favorable way, the proximity of the two becomes less of a free energy penalty; in fact, quite the opposite when the interactions become strong enough. TVs have a surface area to volume ratio almost twice that of OVs. This factor strongly disfavors the TVs in the entropy-dominated case, where monomers avoid the confining surfaces of the crystal. However, in the case where beads and colloids are attractive, a larger surface area per void volume allows beads to interact easily with more colloids than can be achieved if the polymer were located in a more cavernous OV. *When thermal interactions dominate, clearly the arrangement of TVs, rather than OVs, becomes the defining characteristic of each polymorph for an adsorbed polymer.*

If one considers this for the case of  $B_2^* = -1.50$ , the relationship between Fig. 3(b) and Fig. 4 becomes apparent. Figures 4(a) and (b) depict a chain growing in the HCP polymorph under these conditions. While the chain is still sufficiently short ( $M \lesssim 4$ ) the monomers will fill any *single* TV they can find. However, as the chain grows, the HCP polymorph provides a lower free energy environment for the polymer than the FCC, which is accompanied by a change in the number of beads present in the TVs, as evidenced by Fig. 3. Once again, this is a geometric effect, but is now a consequence of the TVs rather than the OVs. Unlike the FCC polymorph, in the HCP crystal pairs of TVs share a common face which allows chains which are too large to fit into a single TV to occupy a pair of them simultaneously. Once again, the HCP provides the polymer with a favorable mode, in this case a TV-TV connection, which is absent in the FCC crystal. A representative snapshot of this configuration is depicted in Figs. 4(a)-(b) when  $M = 6$ . Figure 3(b) reveals that, in the HCP polymorph,  $M_{TV}$  rises linearly until  $M \approx 8$ , whereas in the FCC this persists for only half this length. After filling the TVs, the curves for both the polymorphs plateau as the polymer is forced into an OV (*cf.* Figs. 4(c) and (d)). In the FCC crystal, this begins when  $M \approx 4$  since TVs only share common faces with OVs and vice versa. In the HCP morphology, this is delayed until the second TV fills up. Unlike the OVs which stack indefinitely in the HCP, TVs only share faces between a single pair at a time. This offset of having a pair of TVs initially accessible in only one polymorph shifts the  $M_{TV}$  curve and produces the oscillations in the incremental and overall chemical potential of the polymer. Remarkably,  $\Delta\mu_{tot}^{ex}$  (*cf.* Fig. 3(c)) remains positive over the range of chain lengths we investigated.

When cross interactions are more moderate, there is competition between entropic and energetic effects. At the Boyle point,  $B_2^* = 0.00$  and there is no effective excluded volume between a colloid and a monomer, which calls into question the significance of the voids. Indeed, the lack of any statistically significant difference in Figs. 3(a) and (c) between the polymorphs for all chain lengths confirms that differences in void distributions no longer give rise to differences in polymer chemical potential. Note that the number of monomers occupying the TVs in each polymorph is essentially identical and that the slope in Fig. 3(b) is approximately linear. The HCP polymorph tends to have slightly more monomers in the TVs since they are clustered together, so as the chain grows out of, or in the vicinity of, one it tends to find another TV by chance slightly more often than in the FCC. Note that the slope of  $M_{TV}$  vs.  $M$  is roughly  $1/3$ , which is not insignificant. In a perfect crystal, there are two TVs and one OV

per colloid in both polymorphs. Since a tetrahedron has one quarter the total volume of an octahedron with an identical edge length, the volume fraction encompassed by both TVs is one third of the total in a perfect crystal. A linear slope of this magnitude implies that, when averaged over all polymer configurations in the ensemble, the monomers have an essentially even distribution throughout space. The colloids no longer preclude or bias specific polymer configurations in the ensemble that contribute to this spatial distribution as in the case of  $B_2^* = 1.01$  and  $-1.50$ . Therefore, arranging the colloids in different stacking patterns should have no effect on an adsorbed polymer's free energy, which explains the lack of any statistically significant difference in  $\mu_{\text{tot}}^{\text{ex}}$ . However, we emphasize that an even-handed sampling of the different crystal voids does not imply the polymer is adopting instantaneously ideal configurations under confinement. This would suggest that the ensemble-averaged radius of gyration would scale as  $\langle R_g^2 \rangle^{1/2} \sim M^{1/2}$ . The actual scaling observed suggests that the polymer exists in an extended state as it preferentially exists near the surfaces of the colloids in the crystal with a scaling exponent that falls between that of a rod,  $\nu = 1$ , and that of an unconfined, athermal, three-dimensional chain in a good solvent,  $\nu = 3/5$  (*cf.* Fig. 5). Since the monomer beads are still fully excluded from one another according to eq. 4, regardless of the colloid-monomer interaction, the good solvent exponent is the correct lower bound. Due to the relatively low size asymmetry between the colloids and monomers, our polymer chains are rather short,  $M \lesssim 20$ ; however, an analysis of their scaling behavior reveals reasonable agreement with what would be expected in the limit of very long chains. Our results qualitatively support our analysis of the polymer's behavior under confinement, but we caution the reader that finite-length effects may quantitatively affect the exponents to some degree.

Figure 5 illustrates the ensemble-averaged radius of gyration,  $\langle R_g^2 \rangle^{1/2}$ , for a chain confined in both polymorphs at different  $B_2^*$ . For the purely entropic case where  $B_2^* = 1.01$ , the polymers grow inside large OV's until they reach  $M \approx 10$ . At this point, because the HCP polymorph provides neighboring OV's, the chain can expand directly from one into another whereas the FCC does not provide such an opportunity, prolonging the chain's confinement until it can expand through the tightly confining neighboring TVs which creates the oscillatory patterns depicted.<sup>13</sup> Just before reaching this point, the chain's confinement in the center of the void implies it should scale with an exponent of  $\nu = 1/3$ . Indeed, this is recovered until the chain perforates its OV as illustrated in Fig. 5. However, as energetic effects are introduced, the chain's conformations change dramatically. The favorable colloid-monomer interaction stretches and localizes the chain along the surface of the colloids where previously it was found coiled in the center of one or more voids. This expansion is more dramatic for stronger cross interactions when the chain is short, but appears to converge as the chain becomes much larger (*cf.* Fig. 5(b)). For  $B_2^* = -1.50$  the chain clearly approaches the scaling limit for a two-dimensional self-avoiding random walk ( $\nu = 3/4$ ),<sup>33</sup> which is expected since when energetic interactions are strong, the polymer is expected to traverse the "surface" area of the voids rather than the volume they contain. For both  $B_2^* = 0.00$  and  $-1.50$ , chain conformations appear qualitatively identical in both polymorphs, which is not the case for  $B_2^* = 1.01$ . In the first two cases, the surface localization of the monomers implies they are not as effective at sensing changes on the larger entropic length scale ( $l_s \sim \sigma_c$ ) when a competing energetic length scale ( $l_u \sim \kappa^{-1}$ ) is introduced.

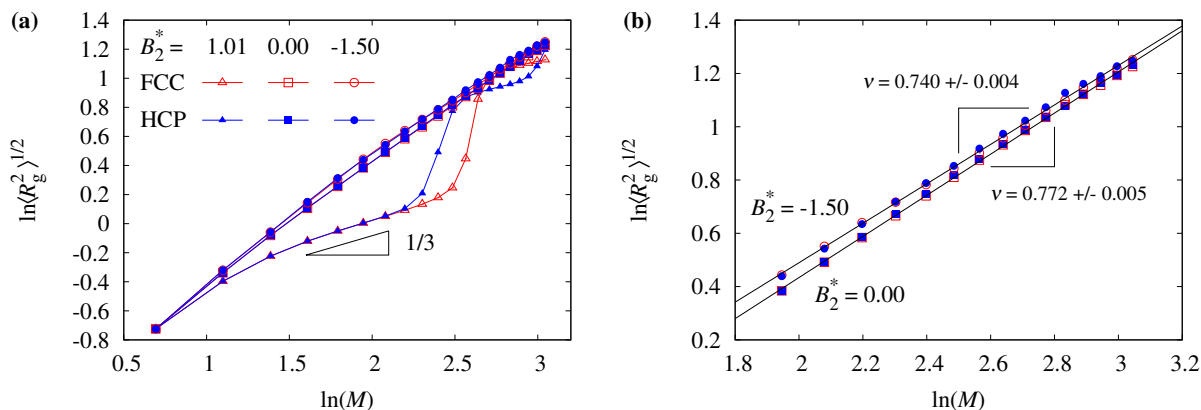


**Fig. 5** (a) Ensemble-averaged radius of gyration for a polymer in a crystal where  $\sigma_c = 6.45$  when the colloid-monomer interaction is such that  $B_2^* = 1.01, 0.00, -1.50$  and  $\kappa^{-1} = 1/5$ . Error bars are always smaller than symbol size so are neglected here. (b) Results for  $B_2^* = 0.00$  and  $-1.50$  which show the change in scaling exponent,  $\nu$ , as the strength of the thermal interaction increases. Standard error as a result of fitting is reported for each exponent.

However, we emphasize that as Fig. 3 illustrates, this does not entirely destroy the polymer's capacity to detect differences in void symmetries since a polymorphic preference re-emerges at very low  $B_2^*$  due to the TVs.

Remarkably, these results suggest that the FCC polymorph will never be more stable than the HCP when in the presence of a homopolymer additive, regardless of the polymer-colloid interaction. Although these simulations do not yield bulk phase diagrams, we previously demonstrated that this MC approach is representative of results obtained from molecular dynamics when  $B_2^* = 1.01$ .<sup>13</sup> However, as  $B_2^*$  decreases we expect kinetic factors to slow the dynamics of these systems making such approaches even less feasible. Previous studies on the structure of polymer-nanoparticle mixtures where the polymer and nanoparticle are thermally interacting have revealed complex many-body interactions leading to a hierarchy of polymer-mediated organization.<sup>25,27,28,34</sup> This includes contact aggregation, which is favorable for first-order phase separations such as crystallization, but also reveals the presence of “bound polymer layers” which tend to stabilize mixtures, though they can still be encouraged to demix at sufficiently low temperatures.<sup>28,34</sup> In fact, like the phenomenon whereby individual crystal polymorphs can be resolved based on chain length, this miscibility window due to adsorbed polymer layers on the surface of the nanoparticles is also dependent on the size of the polymer, and is predicted to narrow as the polymer becomes longer.<sup>34</sup> Our study suggests that for states characterized by close-packed crystal phases in dense polymer-nanoparticle mixtures, the HCP morphology is always more stable than the FCC. The persistence of the HCP stability in the presence of energetic colloid-monomer interactions may help explain why the observation of random hexagonal close-packed crystals, rather than pure FCC crystals as predicted for purely colloidal systems, is so common in experiments on these binary systems.<sup>17</sup>

### 3.2 Mean-field theory for adsorbed, infinitely dilute polymers in polymorphic crystals

From the insight that at  $B_2^* = 0.00$  the polymorph preference disappears, we developed a simplified two-state model for the free energy of a confined polymer by assuming each monomer can exist in one of two possible states defined according to which void type it occupies,  $\nu \in \{\text{OV}, \text{TV}\}$ . We assume that the partition function can be expressed using a monomer's ensemble-averaged location and energy in the crystal:

$$\begin{aligned} q_m &= \sum_{\nu} \Omega(\nu) \exp\left(-\frac{\langle U_{\nu} \rangle}{k_B T}\right) \\ &= \left(\frac{V}{3}\right) \exp\left(-\frac{\langle U_{\text{TV}} \rangle}{k_B T}\right) + \left(\frac{2V}{3}\right) \exp\left(-\frac{\langle U_{\text{OV}} \rangle}{k_B T}\right), \end{aligned} \quad (9)$$

where  $\Omega(\nu)$  is the degeneracy of each void and  $\langle U_{\nu} \rangle$  is the mean energy averaged over the available local configurational space a monomer would have when confined in void  $\nu$ . The entire polymer's partition function can then be expressed by imagining that in the case of  $B_2^* = 0.00$ , the monomers behave as if they were placed independently and randomly throughout space:

$$Q = \frac{q_m^M}{M!} \quad (10)$$

Note that for an ideal gas of monomers,  $\langle U_{\nu} \rangle = 0$  in both void types, so that  $q^{\text{id}} = V$ . Therefore we define  $q_m = q^{\text{id}} q^{\text{ex}}$ , from which the excess free energy follows directly.

$$\frac{F^{\text{ex}}}{k_B T} = -\ln Q^{\text{ex}} = -M \ln q^{\text{ex}} \quad (11)$$

Since  $q^{\text{ex}} = q_m/V$  is just a constant (*cf.* eq. 9) it is clear  $F^{\text{ex}}$  should scale linearly with  $M$ . This prediction is consistent with the results of simulation which reveal that the incremental chemical potential quickly reaches a constant value for  $M > 3$  in Fig. 3. Assuming a finite difference approximation that  $\Delta F/\Delta N \approx \partial F/\partial N = \mu$  at fixed temperature and volume, and since our MC simulations insert a single polymer ( $\Delta N = 1$ ), from Fig. 3(d) we can get the slope of  $\mu_{\text{tot}}^{\text{ex}}/k_B T$  versus  $M$  for  $B_2^* = 0.00$  and obtain an expression for the excess free energy of the adsorbed polymer.

$$\begin{aligned} \frac{\mu_{\text{tot}}^{\text{ex}}}{M k_B T} &= -\ln q^{\text{ex}} \approx -0.227 \\ F^{\text{ex}} &= \langle U_{\text{tot}} \rangle - T S^{\text{ex}} = -0.227 M k_B T \end{aligned} \quad (12)$$

Neglecting relatively small differences between the polymorphs, it is also clear from Fig. 3 that  $\mu_{\text{tot}}^{\text{ex}}$  has an approximately

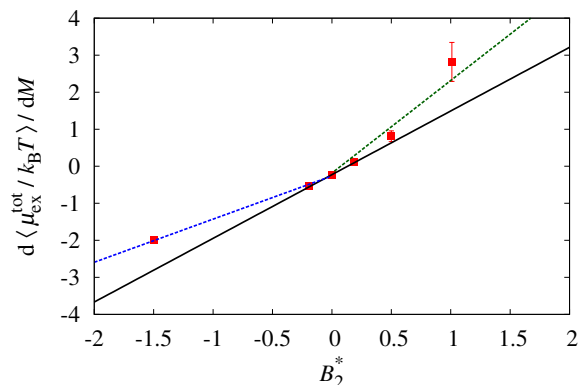


**Fig. 6** The polymorph-averaged slope of the total excess chemical potential versus chain length for an adsorbed homopolymer chain at various  $B_2^*$ . Here  $\sigma_c = 6.45$  and  $\kappa^{-1} = 1/5$  when  $B_2^* < 1.01$ . The standard deviation of the mean incremental chemical potentials taken over  $3 < M < 17$  is reported as the error of the slope, and is only larger than symbol size where indicated. When significant, this error is due to the fact that at a given  $M$  the incremental chemical potential between the polymorphs is very different, rather than uncertainty in the simulations themselves. The dashed lines are only guides to the eye, illustrating the stronger  $B_2^*$  dependence in the entropically-dominated limit (green) and the weaker dependence in the energetically-dominated limit (blue), relative to very near  $B_2^* = 0$  (black).

linear shape for most  $B_2^*$  values as well, despite the fact that the ansatz of eq. 10 is not strictly valid for nonzero  $B_2^*$ . By taking the average  $\mu_i^{\text{ex}}$  between the FCC and HCP crystals at each  $M$  we essentially remove the effect of having different void distributions in each polymorph, resulting in a single mean-field description of a polymorphic close-packed crystal. It is this average that remains approximately linear even when  $\Delta\mu_{\text{tot}}^{\text{ex}}$  is not precisely zero between the polymorphs. The behavior of  $d\langle\mu_{\text{tot}}^{\text{ex}}/k_B T\rangle/dM$ , which is illustrated in Fig. 6, can then be used to extend eq. 12 to other values of  $B_2^*$ . Near  $B_2^* = 0.00$  the slope of  $\langle\mu_{\text{tot}}^{\text{ex}}/k_B T\rangle$  is approximately linear in  $B_2^*$ , which inspires the form:

$$\frac{\langle F^{\text{ex}} \rangle}{Mk_B T} = \left( \frac{\langle F^{\text{ex}} \rangle}{Mk_B T} \right)_{B_2^*=0} + aB_2^* \quad (13)$$

where for this size asymmetry of  $\sigma_c = 6.45$ ,  $a = 1.72$  as depicted by the black line in Fig. 6. Since  $B_2^*$  can be interpreted as an excluded volume between a monomer and colloid, it makes sense that this effective volume should affect  $\langle\mu_{\text{tot}}^{\text{ex}}\rangle$  more strongly in the entropically-dominated limit when  $B_2^* > 0$  than the energetically-dominated limit when  $B_2^* < 0$ , as evidenced by the dashed lines in Fig. 6. While more work is necessary to elucidate a precise form for these corrections, linear approximations above and below  $B_2^* = 0$  show this conclusion is reasonable. Bold black lines in Fig. 3(d) confirm the accuracy of this linearized mean-field expression for polymer free energy confined in a close-packed crystal when  $B_2^*$  is reasonably close to zero.

### 3.3 Role of the interparticle potential

Although the purely repulsive potential between the monomers and colloids produces  $\mu_{\text{tot}}^{\text{ex}}$  curves which appear qualitatively different from those using the Yukawa form in Fig. 3(d), it is more important to understand any qualitative differences in the

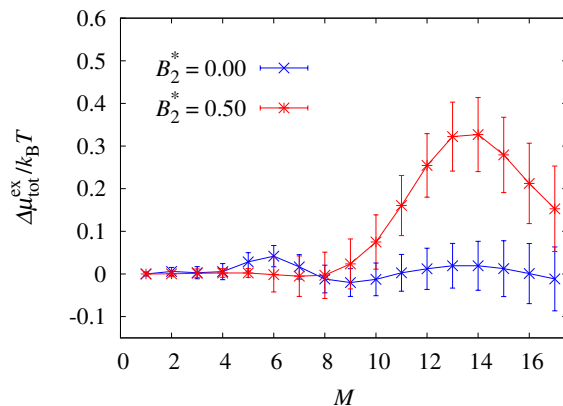


**Fig. 7** Difference in the total excess chemical potential of a polymer adsorbed in each polymorph,  $\Delta\mu_{\text{tot}}^{\text{ex}} = \mu_{\text{tot}}^{\text{ex}}(\text{FCC}) - \mu_{\text{tot}}^{\text{ex}}(\text{HCP})$ , for intermediate values of  $B_2^*$ . Error bars reported here are the standard deviation of at least 10, but for longer chains as many as 30, independent simulations at the same conditions. Since  $\mu_{\text{tot}}^{\text{ex}}$  is a computed from a sum (*cf.* eq. 2), the errors in each term propagate linearly as the chain grows which results in widening error bars as  $M$  increases.

curves of  $\Delta\mu_{\text{tot}}^{\text{ex}}$  in Fig. 3(c). This is because co-solute biasing of a single polymorph relies on the *difference* in the total excess chemical potential of the co-solute between different crystals. Figure 7 compares the results at  $B_2^* = 0.00$  and 0.50 employing the attractive Yukawa potential. Clearly at  $B_2^* = 0.00$ , despite some apparent oscillations, the curve does not deviate from zero in a statistically significant fashion, and thus, we conclude the two crystal polymorphs provide equally stable environments for an adsorbed polymer. However, as  $B_2^*$  increases, these oscillations give way to a curve which qualitatively resembles that in Fig. 3(c) for  $B_2^* = 1.01$ . Since the same shape of the  $\Delta\mu_{\text{tot}}^{\text{ex}}$  curve obtained with the purely repulsive potential is recovered with the attractive Yukawa form for  $B_2^* > 0$ , using  $B_2^*$  to distinguish between the entropically ( $B_2^* > 0$ ) and energetically dominated ( $B_2^* < 0$ ) cases is qualitative robust against a specific form of the interparticle potential.

Despite this, quantitative differences do exist as  $\sigma_c$ ,  $\kappa^{-1}$ , and  $\epsilon$  change which cannot be isomorphically reduced in terms of  $B_2^*$  to relate how changes in one can be precisely compensated by changes to one or more of the others. These differences are easiest to discuss within the framework of the mean-field theory outlined in the previous section. Figure 8(a) depicts the asymptotic polymorph-averaged slope of  $\mu_{\text{tot}}^{\text{ex}}$  as the chain grows for increasing colloid diameter at different  $B_2^*$  and  $\kappa^{-1}$ . Tabulated values and simulation conditions for this figure can be found in the SI. For a fixed  $B_2^*$  and  $\sigma_c$ , decreasing  $\kappa^{-1}$  decreases the range of the attractive interaction between the colloids and monomers. To maintain a constant  $B_2^*$ ,  $\epsilon$  is concomitantly increased. Together these changes draw the monomers closer to the surface of the colloids out of the center of the voids. This reduces the amount of favorable many-body interactions a monomer may have with multiple colloids relative to a system with a larger  $\kappa^{-1}$ , lowering the magnitude of its overall energy (which since it is attractive, is negative) leading to an increase in  $\langle\mu_i^{\text{ex}}/k_B T\rangle = d\langle\mu_{\text{tot}}^{\text{ex}}/k_B T\rangle/dM$ . For all fixed  $\sigma_c$  and  $\kappa^{-1}$ , changing  $\epsilon$  ( $B_2^*$ ) alone produces an approximately linear shift in  $\langle\mu_i^{\text{ex}}\rangle$  which is consistent with the linear form of eq. 13. However, the most pronounced feature of Fig. 8(a) is the apparent plateau as  $\sigma_c$  is increased. The fact that this plateau occurs regardless of  $B_2^*$  or  $\kappa^{-1}$  is strong evidence that another factor, identical in all of these cases, is responsible.

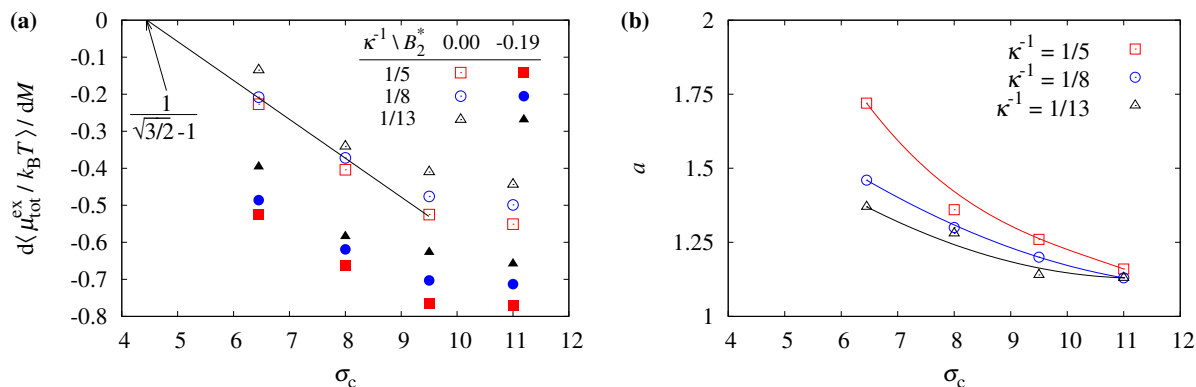


**Fig. 8** (a) Asymptotic slope of the polymorph-averaged total excess chemical potential against  $M$  for various colloid diameters,  $\sigma_c$ , at two different  $B_2^*$  values. Three ranges,  $\kappa^{-1}$ , are investigated where the strength,  $\epsilon$ , has been adjusted to keep  $B_2^*$  constant. Filled symbols correspond to  $B_2^* = -0.19$ , while open ones refer to  $B_2^* = 0.00$ . (b) Mean-field parameter,  $a$ , from eq. 13 for various  $\kappa^{-1}$  and  $\sigma_c$ . Lines serve as a guide to the eye.

In fact, this common thread is the monomers themselves.

We performed simulations such that  $\sigma_c/\sigma_m \geq 6.45$  because otherwise monomers growing on a chain could not escape their initial void cavity as they would be too large to fit through tangent triplets of colloids forming the crystal. However, if we nonetheless extrapolate the apparently linear slope to small  $\sigma_c$  for the case of  $B_2^* = 0.00$  (black line in Fig. 8(a)) the intercept occurs at  $\sigma_c = 1/(\sqrt{3/2} - 1) \approx 4.45$ . At this size, a single monomer can just fit into a TV, and an OV is not quite large enough to accommodate a dimer. So the crystal can only provide space for a polymer composed of a single monomer unit which, at  $B_2^* = 0.00$ , should have no net excluded volume with the colloids. This is the reason the excess chemical potential is zero at this point. As the colloid diameter increases, the crystal can accommodate longer polymers, though under such confinement their monomers are strongly influenced by packing effects with other monomers since in our model they always remain purely repulsive with one another. However, as the asymmetry increases, these monomer-level packing effects are alleviated leading to the observed plateau around  $\sigma_c \geq 9.50$ . In previous work these effects led to a similar plateau in  $\Delta\mu_{\text{tot}}^{\text{ex}}$  at approximately the same asymmetry when  $B_2^* = 1.01$ , further supporting this conclusion.<sup>13</sup> This is also consistent with the scaling exponents recovered in Fig. 5 which suggest a two-dimensional *self-avoiding* random walk at large  $M$ .

The fact that the chemical potentials initially become negative as  $\sigma_c$  increases beyond roughly 4.45, even though  $B_2^* = 0.00$ , is a result of spatial correlation as a consequence of monomer bonds. In close-packed crystals, the tangency of colloids implies that, even if the monomers interact only at contact in a “sticky hard-sphere” fashion, a single monomer can always be placed mutually tangent to two colloids which are, themselves, tangent. This three-body effect lowers the energy of the system substantially compared to the case of simple two-body interaction. For systems with a finite range of interaction these three-body interactions can occur more frequently. Moreover, for chains of a length  $M \geq 2$  the energetic favorability of locations which benefit from three-body interactions imply that once a monomer inhabits such a region, there is a disproportionate increase in the likelihood

---

that neighboring monomers, which are topologically constrained to the local neighborhood, will also benefit from such effects. This combination of local spatial correlations enhancing many-body interactions lowers the system's energy, and thus the polymer chemical potential, relative to that of a system of unbonded monomers (with no topological correlations). Of course packing effects at lower  $\sigma_c$  initially oppose this trend, until they are completely alleviated at higher  $\sigma_c$  leaving only the consequence of these many-body thermal interactions behind; hence, the shape of the curves in Fig. 8(a). However, although both  $\kappa^{-1}$  and  $\sigma_c$  have independent consequences on the mean-field free energy of the adsorbed polymer, we find that the corrections to eq. 13 collapse for both these parameters. Figure 8(b) illustrates that as  $\sigma_c$  increases, the mean-field parameter,  $a$ , approaches unity implying the equation of state (*cf.* eq. 13) is completely captured with only the first order correction of  $B_2^*$  for all  $\kappa^{-1}$  and  $\sigma_c$ .

## 4 Conclusions

We studied the relative stability of the hexagonal close-packed (HCP) and face-centered cubic (FCC) colloidal crystals in the presence of linear homopolymers, whose segments interact energetically with the crystal, using Monte Carlo simulations. This significantly extends prior work that only examined the case of purely athermal monomer-colloid interactions. We find that the reduced second virial coefficient,  $B_2^*$ , serves as a powerful order parameter separating qualitatively different regimes governed primarily by entropic or energetic effects, according to the sign of  $B_2^*$ . In all cases, the HCP crystal provides an equal or lower free energy environment for an adsorbed polymer than its FCC counterpart. In the case where  $B_2^* < 0$ , thermal interactions outweigh entropic penalties driving the monomers into the smaller TVs. Since the HCP crystal has face-sharing pairs of TVs, a polymer benefits from being able to distribute itself across multiple voids when the chain becomes very long, whereas in the FCC crystal these pairs do not exist. In the opposite case when entropy dominates the system,  $B_2^* > 0$ , the face-sharing OV's which are only present in the HCP, provide a similar effect. In both cases, it is the nature of the HCP polymorph, which arranges similar voids near each other, that creates a lower free energy environment for an adsorbed polymer than in the FCC crystal. This work demonstrates that the previously elucidated polymer-mediated control over polymorph stability is extendable from the limiting case of athermal colloid-monomer interactions to more experimentally realizable scenarios where the polymers and colloids have a finite range of interaction. The predictions made here are premised on the behavior of a single polymer adsorbed in the crystal phase, which is a reasonable approximation when the adsorbed polymer is somewhat dilute inside the crystal. However, studying the effect of concentration inside the crystal phase is an important subject for future investigation. Furthermore, although our current methodology relies on an equilibrium thermodynamic approach, kinetic and ergodicity factors are also plausible routes to producing a specific polymorph. This is the subject of ongoing and future work.

---

## 5 Acknowledgements

This publication was supported by collaborative research grants CBET-1403049 (Princeton) and CBET-1402166 (Columbia) from the US National Science Foundation.

## References

- 1 L. V. Woodcock, *Nature*, 1997, **385**, 141–143.
- 2 P. G. Bolhuis, D. Frenkel, S.-C. Mau and D. A. Huse, *Nature*, 1997, **388**, 235–236.
- 3 S.-C. Mau and D. A. Huse, *Physical Review E*, 1999, **59**, 4396–4401.
- 4 T. C. Hales, *Annals of Mathematics*, 2005, **162**, 1065–1185.
- 5 S. Pronk and D. Frenkel, *Journal of Chemical Physics*, 1999, **110**, 4589–4592.
- 6 S. Auer and D. Frenkel, *Nature*, 2001, **413**, 1020–1023.
- 7 P. N. Pusey, E. Zaccarelli, C. Valeriani, E. Sanz, W. C. K. Poon and M. E. Cates, *Philosophical Transactions of the Royal Society A*, 2009, **367**, 4993–5011.
- 8 V. J. Anderson and H. N. W. Lekkerkerker, *Nature*, 2002, **416**, 811–815.
- 9 J. Zhu, M. Li, R. Rogers, W. Meyer, R. H. Ottewill, S.-S. S. Crew, W. B. Russel and P. M. Chaikin, *Nature*, 1997, **387**, 883–885.
- 10 E. A. Kamenetzky, L. G. Magliocco and H. P. Panzer, *Science*, 1994, **263**, 207–209.
- 11 I. I. Tarhan and G. H. Watson, *Physical Review Letters*, 1996, **76**, 315–318.
- 12 S. Furumi, *Journal of Materials Chemistry C*, 2013, **1**, 6003–6012.
- 13 N. A. Mahynski, A. Z. Panagiotopoulos, D. Meng and S. K. Kumar, *Nature Communications*, 2014, **5**, 1–8.
- 14 D. Frenkel, *Physica A*, 1999, **263**, 26–38.
- 15 M. Dijkstra, R. van Roij and R. Evans, *Physical Review Letters*, 1999, **82**, year.
- 16 H. N. W. Lekkerkerker and R. Tuinier, *Colloids and the Depletion Interaction*, Springer, 2011, vol. 833.
- 17 E. H. A. de Hoog, W. K. Kegel, A. van Blaaderen and H. N. W. Lekkerkerker, *Physical Review E*, 2001, **64**, 021407.
- 18 W. C. K. Poon, *Journal of Physics: Condensed Matter*, 2002, **14**, R859–R880.
- 19 P. G. Bolhuis, A. A. Louis and J. P. Hansen, *Physical Review Letters*, 2002, **89**, 128302.
- 20 M. Schmidt, A. R. Denton and J. M. Brader, *Journal of Chemical Physics*, 2003, **118**, 1541–1549.
- 21 R. L. C. Vink and M. Schmidt, *Physical Review E*, 2005, **71**, 051406.
- 22 T. W. Rosch and J. R. Errington, *Journal of Chemical Physics*, 2008, **129**, 164907.
- 23 A. Fortini, P. G. Bolhuis and M. Dijkstra, *Journal of Chemical Physics*, 2008, **128**, 024904.
- 24 J. B. Hooper, K. S. Schweizer, T. G. Desai, R. Koshy and P. Keblinski, *Journal of Chemical Physics*, 2004, **121**, 6986–6997.
- 25 J. B. Hooper and K. S. Schweizer, *Macromolecules*, 2005, **38**, 8858–8869.
- 26 J. Liu, Y. Gao, D. Cao, L. Zhang and Z. Guo, *Langmuir*, 2011, **27**, 7926–7933.
- 27 S. Y. Kim, K. S. Schweizer and C. F. Zukoski, *Physical Review Letters*, 2011, **107**, 225504.
- 28 S. Y. Kim and C. F. Zukoski, *Langmuir*, 2011, **27**, 10455–10463.
- 29 V. Ganesan and A. Jayaraman, *Soft Matter*, 2014, **10**, 13–38.
- 30 S. K. Kumar, I. Szleifer and A. Z. Panagiotopoulos, *Physical Review Letters*, 1991, **66**, 2935–2938.
- 31 G. S. Grest and K. Kremer, *Physical Review A*, 1986, **33**, 3628–3631.

- 
- 32 D. Frenkel and B. Smit, *Understanding Molecular Simulation*, Academic Press, 2002, vol. 1.
  - 33 M. Rubinstein and R. H. Colby, *Polymer Physics*, Oxford University Press, 2003.
  - 34 J. B. Hooper and K. S. Schweizer, *Macromolecules*, 2006, **39**, 5133–5142.

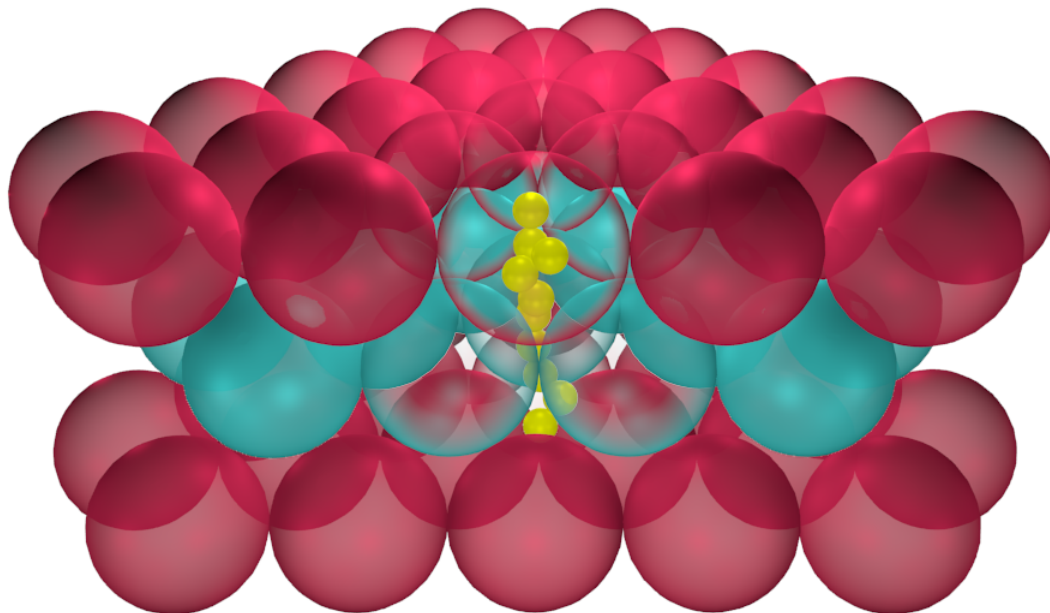


**Figure 1:** A linear polymer (in yellow) adsorbed in the voids of a hexagonal close-packed crystal. Three crystal layers, ABA, are depicted in alternating colors of red and cyan.